

## Understanding the adsorption of benzimidazole derivative as corrosion inhibitor for carbon steel in 1 M HCl: Experimental and theoretical studies

Y. El Aoufir<sup>1,2\*</sup>, Y. El Bakri<sup>3</sup>, H. Lgaz<sup>1,4</sup>, A. Zarrouk<sup>5</sup>, R. Salghi<sup>4</sup>, I. Warad<sup>6</sup>,  
Y. Ramli<sup>7</sup>, A. Guenbour<sup>2</sup>, E.M. Essassi<sup>3</sup>, H. Oudda<sup>1</sup>

<sup>1</sup> Laboratory of Separation Processes, Faculty of Sciences, University Ibn Tofail, Kenitra, Morocco

<sup>2</sup> Laboratory of Nanotechnology, Materials & Environment, Faculty of Sciences, Mohammed V University, Rabat, Morocco

<sup>3</sup> Laboratoire de chimie organique heterocyclique, URAC 21, Pôle de compétence pharmacochimie, Université Mohammed V, Faculté des sciences, Rabat, Maroc

<sup>4</sup> Laboratory of Applied Chemistry & Environment, ENSA, Ibn Zohr University, PO Box 1136, 80000 Agadir, Morocco

<sup>5</sup> LC2AME, Faculté des Sciences, Université Mohammed 1<sup>er</sup>, Oujda, Morocco

<sup>6</sup> Department of Chemistry, AN-Najah National University P.O. Box 7, Nablus, Palestine.

<sup>7</sup> Medicinal Chemistry Laboratory, Faculty of Medicine and Pharmacy, Mohammed V University Rabat, 10170 Rabat, Morocco

Received 14 Jan 2017,  
Revised 05 May 2017,  
Accepted 11 May 2017

### Keywords

- ✓ Carbon steel ;
- ✓ Hydrochloric acid
- ✓ Corrosion inhibition ;
- ✓ Benzimidazole derivative
- ✓ Electrochemical techniques ;
- ✓ DFT ;

Y. El Aoufir  
[evasmina1@gmail.com](mailto:evasmina1@gmail.com)  
0661183348

### Abstract

The inhibition performance of 5-methoxy-2-[(4-methoxy-3,5-dimethyl-pyridin-2-yl)methylsulfanyl]benzimidazole (MSB) on the corrosion of carbon steel in 1M HCl was investigated using electrochemical impedance spectroscopy (EIS) and potentiodynamic measurements at various concentrations. It was found that tested compound has high inhibitory efficiency against the corrosion of carbon steel in HCl solution. The inhibition efficiency increases with concentration and decreases a little with the rises of the temperature from 303 to 333 K. Results showed that MSB shows maximum inhibition efficiency of 95% at 10<sup>-3</sup> M concentration. This compound is classified as the mixed type corrosion inhibitor with predominant control of cathodic reaction. The adsorption of benzimidazole derivative on the surface of carbon steel obeyed the isotherm of Langmuir adsorption. Quantum chemical calculations were employed to give further insight into the mechanism of inhibition action of MSB.

## 1. Introduction

It is a well-known fact that acids are used in various operations, such as industrial acid cleaning, acid descaling, and oil well acidification [1-5]. In these corrosive media, organic inhibitors are often used to lessen the rate of metal corrosion. The inhibitory efficiency of organic molecules mainly depends on their adsorption ability on metal surface, which can markedly change the corrosion resisting properties of metals [6-10]. Generally, the most efficient inhibitor molecules contain nitrogen, sulfur, oxygen, multiple bonds and aromatic rings [11-26]. Benzimidazole, a heterocyclic aromatic organic compound, consists of the fusion of benzene and imidazole. The nitrogen atom and the aromatic ring in molecular structure are likely the facilitator of the adsorption of benzimidazole on the metallic surface [27-30]. However, relatively high concentration of benzimidazole is essential to achieve effective inhibition for steel in acidic medium. At the concentration of 10 mM, typically, the inhibition efficiency of benzimidazole for carbon steel in 1M HCl is only around 50% [31,32]. In hope of improving the inhibition effectiveness of benzimidazole, researchers have made a lot of attempts to develop new benzimidazole derivatives.

In the present work, we attempt to prepare a new benzimidazole derivative, 5-methoxy-2-[(4-methoxy-3,5-dimethyl-pyridin-2-yl)methylsulfanyl]benzimidazole (MSB) and to evaluate its corrosion inhibition for carbon steel in 1M HCl. The electrochemical impedance spectroscopy (EIS) and polarization measurements were used for clarification of corrosion and adsorption behavior. The thermodynamic and kinetic parameters were determined and discussed.

## 2. Experimental details

### 2.1. Synthesis of the benzimidazole derivative used as corrosion inhibitor

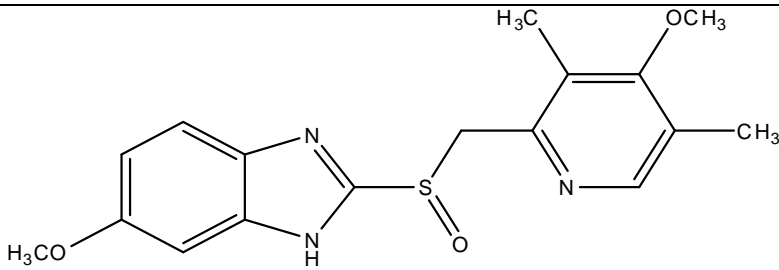
Omeprazole the “substituted benzimidazole”; is a covalent class of PPIs (Proton Pump Inhibitors); inhibits the pump by irreversibly binding to cysteines in the pump. The irreversibility of the covalent bond results in inhibition of acid secretion until more enzymes are synthesized i.e. inhibition of enzymes H<sup>+</sup>/K<sup>+</sup>-ATPase [Hydrogen–Potassium Adenosine Triphosphates] at the secretory surface of the gastric parietal cell. This effect leads to inhibition of both basal and stimulated acid secretion, irrespective of the stimulus, for more than 24 h [33-35]. The compound was characterized by N.M.R. <sup>1</sup>H-NMR (DMSO-d<sub>6</sub>) (δ ppm): 2.31(s,3H,CH<sub>3</sub>), 2.81(s,1H,CH), 3.83(s,3H;O-CH<sub>3</sub>), 6.93(d,1H,CH<sub>aromatique</sub>), 7.48(d,1H, CH<sub>aromatique</sub>) 8.41(s,1H,CH-N).

<sup>13</sup>C-NMR (DMSO-d<sub>6</sub>) (δ ppm): 15.7(CH<sub>3</sub>), 55.8(O-CH<sub>3</sub>), 56.8(CH<sub>2</sub>), 100.8(C<sub>aromatique</sub>), 115(C-CH<sub>3</sub>), 116.2(C<sub>aromatique</sub>), 131.2(C-N), 158.5(C=N).

### 2.2. Material preparation and inhibitors

The chemical formula of inhibitor is grouped in the Table.1. The concentrations tested ranges between 10<sup>-3</sup> and 10<sup>-6</sup> M. Corrosive solutions were prepared by dilution of an analytical reagent grade 37% HCl with doubly distilled water.

**Table 1.** Names and chemical structures of the organic compounds investigated

Abbreviation	Structural formula
MSB	 <p>5-methoxy-2-[(4-methoxy-3,5-dimethyl-pyridin-2-yl)methylsulfanyl]benzimidazole</p>

Corrosion tests have been carried out on electrodes cut from sheets of carbon steel. Steel strips containing 0.36 wt.% C, 0.66 wt.% Mn, 0.27 wt.% Si, 0.02 wt.% S, 0.015 wt.% P, 0.21 wt.% Cr, 0.02 wt.% Mo, 0.22 wt.% Cu, 0.06 wt.% Al and the rest iron.

The working area of 1 cm<sup>2</sup> was subsequently ground with 180 and 1500 grit grinding papers, cleaned by distilled water and ethanol at hot air. The effect of temperature on the inhibition efficiencies for the inhibitor was tested between 303 and 333 K.

### 2.3. Electrochemical measurements

Electrochemical measurements, including stationary methods (PDP) and transient (EIS) were performed in a three-electrode cell. Pure carbon steel specimen was used as the working electrode, a saturated calomel (SCE) as reference and an area platinum as counter electrode (CE) were used. All potentials were measured against SCE. The working electrode was immersed in a test solution for 30 min until the corrosion potential of the equilibrium state ( $E_{corr}$ ) was achieved using a type PGZ100 potentiostat. The potentiodynamic polarization curves were determined by a constant sweep rate of 1 mv/ s. The measurements of the transitory method (EIS) were determined, using ac signals of amplitude 10 mV peak to peak at different conditions in the frequency range of 100 kHz to 10 mHz. The data obtained by EIS method were analyzed and fitted using graphing and analyzing impedance software, version Zview2. The inhibition efficiency of the studied compound was calculated using the following equation:

$$\eta_{PDP}(\%) = \left[ 1 - \frac{i_{corr}}{i_{corr}^{\circ}} \right] \times 100 \quad (1)$$

where  $i_{corr}$  and  $i_{corr}^{\circ}$  are the corrosion rates in the presence and absence of inhibitor, respectively. The impedance diagrams were determined by EIS method. To confirm reproductibility, all experiments were repeated three times and the evaluated inaccuracy does not exceed 10%. The inhibition efficiency was calculated using the following equation:

$$\eta_z(\%) = \frac{R_p - R_{p(i)}}{R_{p(i)}} \times 100 \quad (2)$$

where  $R_p$  and  $R_{p(i)}$  were the polarisation resistance of carbon steel electrode in the uninhibited and inhibited solutions, respectively.

#### 2.4. Density Functional Theory (DFT)

Quantum chemical calculations were performed using density functional theory (DFT) with the Beck's three parameter exchange functional along with the Lee-Yang-Parr non local correlation functional (B3LYP) [36,37] with 6-31G (d, p) basis set is implemented in Gaussian 09 program package [36]. This approach is shown to yield favorable geometries for a wide variety of systems. The following quantum chemical parameters were evaluated from the optimized molecular structure: the energy of the highest occupied molecular orbital ( $E_{HOMO}$ ), the energy of the lowest unoccupied molecular orbital ( $E_{LUMO}$ ), the energy band gap ( $\Delta E_{gap} = E_{HOMO} - E_{LUMO}$ ) and the number of transferred electrons ( $\Delta N$ ).

#### 2.5. Molecular dynamic simulation

The Monte Carlo (MC) search was adopted to compute the low configuration adsorption energy of the interactions of the MSB on a clean iron surface. The Monte Carlo (MC) simulation was carried out using Materials Studio 5.0 software (Accelrys, Inc.) [38]. The Fe crystal was cleaved along the (110) plane, it is the most stable surface as reported in the literature. Then, the Fe (110) plane was enlarged to (12×12) supercell to provide a large surface for the interaction of the inhibitor. The simulation of the interaction between MSB and the Fe (110) surface was carried out in a simulation box ( $29.78 \times 29.78 \times 60.13 \text{ \AA}$ ) with periodic boundary conditions, which modeled a representative part of the interface devoid of any arbitrary boundary effects. After that, a vacuum slab with 30 Å thickness was built above the Fe (110) plane. All simulations were implemented with the COMPASS force field to optimize the structures of all components of the system of interest. More simulation details on the methodology of Monte Carlo simulations can be found in previous publications [39-41].

### 3. Results and discussion

#### 3.1. Polarization results

The representative potentiodynamic polarization curves of the carbon steel electrode, which were obtained in 1M HCl solution in the absence and presence of various concentrations of benzimidazole derivative, are given in Fig. 1. In order to obtain information about the kinetics of the corrosion, some electrochemical parameters, *i.e.*, corrosion potential ( $E_{corr}$ ), corrosion current density ( $i_{corr}$ ) cathodic ( $\beta_c$ ) and anodic ( $\beta_a$ ) Tafel slopes and inhibition efficiency ( $\eta_{PDP}$  %) values were calculated from the corresponding polarization curves and the obtained data are given in Table 2.

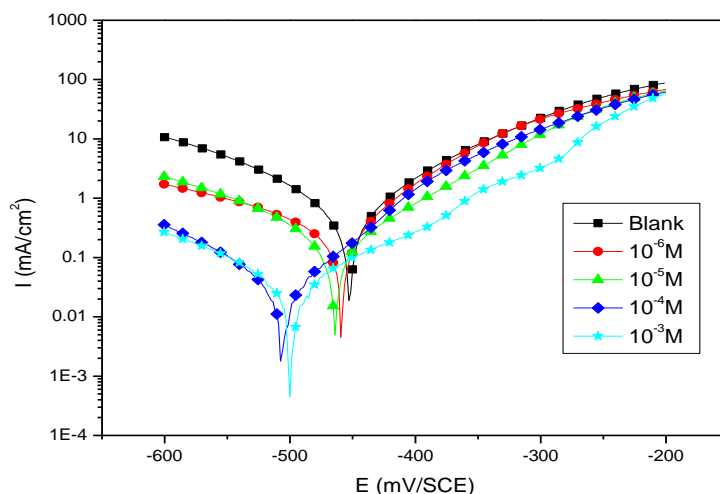


**Figure 1:** Potentiodynamic polarization curves for carbon steel in 1M HCl solution in the presence and absence of different concentrations of MSB at 303 K.

**Table 2.** The electrochemical parameters calculated by the potentiodynamic polarization technique for the corrosion of CS in 1 M HCl in the absence and presence of different concentrations of MSB at 303 K.

Medium	Conc (M)	$-E_{\text{corr}}$ (mV/SCE)	$I_{\text{corr}}$ ( $\mu\text{A cm}^{-2}$ )	$\beta_a$ (mV dec $^{-1}$ )	$-\beta_c$ (mV dec $^{-1}$ )	$\eta$ (%)
HCl	1	452	507	100	122	—
MSB	$10^{-6}$	459	148	101	82	71
	$10^{-5}$	463	88	90	112	83
	$10^{-4}$	506	45	104	105	91
	$10^{-3}$	499	32	106	103	94

It can be noticed that the curves shift towards lower current density region in the presence of the inhibitor compared to the blank acid medium. This suggests that the studied compound reduce the corrosion current and therefore reduce the corrosion rate. The suppression effect becomes more pronounced with the increase of the concentration of inhibitor. The polarization curves also exhibit shifts in potential towards more cathodic regions relative to the acid blank.

We can classify an inhibitor as cathodic or anodic type if the displacement in corrosion potential is more than 85 mV with respect to corrosion potential of the blank [6,7]. In the presence of inhibitor, the corrosion potential of carbon steel shifted to the negative side only 54 mV (vs. SCE) for MSB. This can be interpreted that tested inhibitor acts as a mixed type inhibitor and shows more pronounced influence in the cathodic polarization plots compared to that in the anodic plots. The data in Table 2 reveals that when the concentration of MSB increased, the inhibition efficiency increases and the corrosion current density decreases sharply. This may be due to the adsorption layer of the inhibitor on the metal surface.

### 3.2. Electrochemical impedance spectroscopy (EIS)

The Nyquist plots recorded for carbon in 1 M HCl in the inhibitor-free solution and in the presence of various concentrations of benzimidazole derivative is shown in Fig. 2. Inspection of the Fig. 2 showed that diameters of the Nyquist plots increase on increasing concentrations of MSB which attributed due to their adsorption on metal/ electrolyte interfaces [42-44]. In the Nyquist plots, the subtraction of lower frequency from the higher frequency of the real impedance is defined as charge transfer resistance ( $R_{ct}$ ). However, in our present case polarization resistance ( $R_p$ ) has been used at the place of charge transfer resistance ( $R_{ct}$ ).

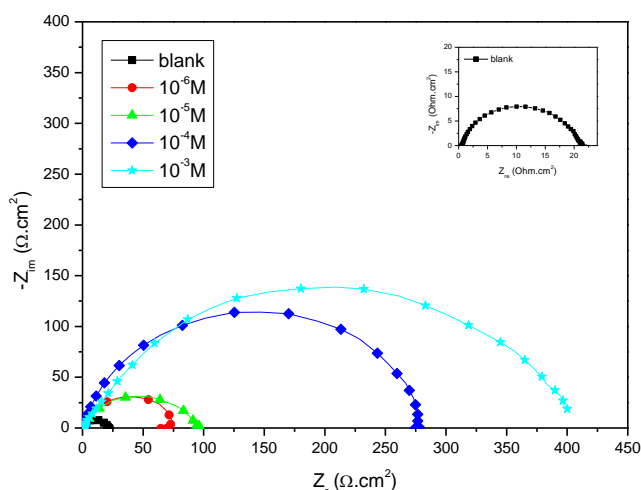


**Figure 2:** Nyquist plots for carbon steel in 1 M HCl solution containing various concentrations of MSB at 303 K.

Generally,  $R_p$  includes resistance due to accumulation of corrosion products (rust and scales) at metal/electrolyte interfaces i.e. accumulation resistance ( $R_a$ ), resistance due to adsorption of inhibitors at metal/ electrolyte interfaces i.e. film resistance ( $R_f$ ), and diffusion layer resistance ( $R_d$ ) in addition to the charge transfer resistance ( $R_{ct}$ ) i.e.  $R_p = R_{ct} + R_a + R_f + R_d$  [45-47]. Several electrochemical impedance parameters such as solution

resistance ( $R_s$ ), polarization resistance ( $R_p$ ), phase shift ( $n$ ), double layer capacitance ( $C_{dl}$ ) and percentage of inhibition efficiency were derived with the help of an equivalent circuit as described elsewhere [45,46] and are depicted in Table 3. In acid solution metal surface becomes inhomogeneous due to corrosion; therefore, to compensate the surface inhomogeneity, constant phase element (CPE) has been used at the place of pure capacitor [42]. The impedance of the CPE ( $Z_{CPE}$ ) can be derived using following equation:

$$Z_{CPE} = \frac{1}{Q(j\omega)^n} \quad (3)$$

where,  $Q$  is the CPE constant (in  $\Omega^{-1} S^n cm^{-2}$ ),  $\omega$  is the angular frequency (in  $rad s^{-1}$ ),  $j^2 = -1$  is the imaginary number and  $n$  is a CPE exponent which can be used as a gauge for the heterogeneity or roughness of the surface [48,49]. In addition, the double layer capacitances,  $C_{dl}$ , for a circuit including a CPE were calculated by using the following Eq. 4:

$$C_{dl} = (Q \times R^{1-n})^{\frac{1}{n}} \quad (4)$$

The impedance spectra were fitted to the  $R_s(R_p/CPE)$  equivalent circuit of the form in Fig. 3.

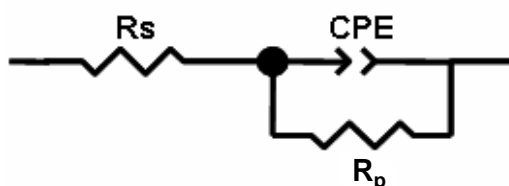


**Figure 3:** Equivalent electrical circuit corresponding to the corrosion process on the carbon steel in hydrochloric acid.

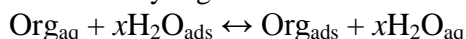
A careful inspection of the results depicted in the Table 3 shows that the values of  $R_p$  increase and that of  $C_{dl}$  decrease with increase in the inhibitor concentration which results in an increased thickness of electric double layer due to adsorption of inhibitor molecules on the metallic surface and/ or decreased value of dielectric constant due to replacement of water molecules by the inhibitor [50,51].

**Table 3.** Impedance parameters recorded for carbon steel electrode in 1M HCl solution in the absence and presence of different concentrations of inhibitor at 303K.

Medium	Conc (M)	$R_s$ ( $\Omega cm^2$ )	$R_p$ ( $\Omega cm^2$ )	$10^{-4}Q$ ( $\Omega^{-1}cm^{-2}s^{-n}$ )	$n$	$C_{dl}$ ( $\mu F cm^{-2}$ )	$\eta_z$ (%)
Blank	1	0.568	20.24	2.420	0.860	112	-
MSB	$10^{-6}$	1.636	76.31	1.640	0.8109	59	74
	$10^{-5}$	1.336	90.81	1.430	0.7814	42	78
	$10^{-4}$	1.343	276.80	0.6515	0.8681	34	93
	$10^{-3}$	0.848	404.90	0.623	0.7852	22	95

### 3.3. Adsorption isotherm

The adsorption of organic molecules at the metal/solution interface consists of the replacement of water molecules by organic molecules according to following process [52].



where  $Org_{(aq)}$  and  $Org_{(ads)}$  are organic molecules in the solution and adsorbed on the metal surface, respectively, and  $x$  is the number of water molecules replaced by the organic molecules. The inhibitory efficiencies of the organic molecules mainly depend on their adsorption ability on the metal surface. Therefore, the determination of relation between adsorption and corrosion inhibition is of great importance. In order to clarify the nature and the strength of the adsorption of tested inhibitor on carbon steel, the experimental results were fitted to a series of adsorption isotherms, *i.e.*, Langmuir, Temkin and Frumkin. The best description of the adsorption behavior of studied inhibitor is explained by Langmuir adsorption isotherm, which is given by Eq. 5[53].

$$\frac{C_{inh}}{\theta} = \frac{1}{K_{ads}} + C_{inh} \quad (5)$$

where  $C_{inh}$  is the concentration of inhibitor and  $K_{ads}$  the adsorptive equilibrium constant.

Fig. 4 shows the curves of the variation of  $C_{inh}/\theta$  according to the concentration  $C_{inh}$  for the benzimidazole compound. The values of  $K_{ads}$  obtained from the reciprocal of intercept of Langmuir isotherm line are listed in Table 4, together with the values of the Gibbs free energy of adsorption  $\Delta G_{ads}^\circ$  calculated from the equation[53]:

$$K_{ads} = \left(\frac{1}{55.5}\right) \exp\left(-\frac{\Delta G_{ads}^\circ}{RT}\right) \quad (6)$$

where R is gas constant, T is absolute temperature of experiment and the constant value of 55.5 is the concentration of water in solution.

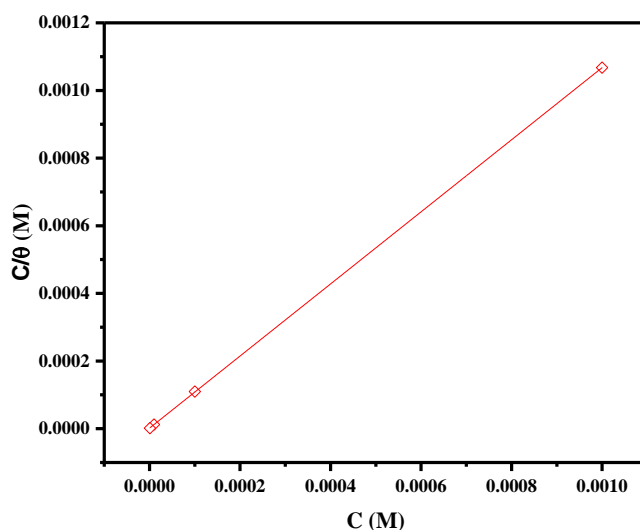


**Figure 4:** Langmuir adsorption of inhibitor on the CS surface in 1.0 M HCl solution at 303K.

The high value of adsorption equilibrium constants  $K_{ads}$  correspondent's benzimidazole compound to reflect the high adsorption capacity of this inhibitor on the surface of carbon steel in acidic 1 M HCl [3]. This suggests that this inhibitor can best recoveries, where it is most effective protection against corrosion. The  $\Delta G_{ads}^\circ$  values are negative and high ( $-43.7 \text{ kJ mol}^{-1}$ ) indicates the strong interactions between the inhibitor molecules and the metal surface[54-56]. Literature study reveals that the value of  $\Delta G_{ads}^\circ$  up to  $-20 \text{ kJ/mol}$  or less negative is related to the electrostatic interactions between inhibitor and metallic surfaces (physisorption), while the value of  $\Delta G_{ads}^\circ$  is around  $-40 \text{ kJ/mol}$  or more negative related to the charge sharing between inhibitor and metallic surfaces (chemisorption) [53]. However, in our present case the value of  $\Delta G_{ads}^\circ$  suggest that adsorption of the benzimidazole on carbon steel surface follows chemisorption mode [53].

**Table 4.** The values of  $K_{ads}$  and  $\Delta G_{ads}^\circ$  for carbon steel in presence of MSB in 1 M HCl at 303 K.

Inhibitor	$R^2$	$K_{ads}$ (L/mol)	$\Delta G_{ads}^\circ$ (kJ/mol)
MSB	0.9999	627313	-43.7

### 3.4. Effect of the temperature

The temperature can modify the interaction between the steel electrode in acidic medium in the absence and presence of the inhibitor[57]. In order to study the effect of temperature on the inhibition efficiencies of the benzimidazole compound, polarization experiments were conducted in the range of 303–333 K, in the absence and presence of  $1 \times 10^{-3} \text{ M}$  of inhibitor (Fig. 5). The values of corrosion potential ( $E_{corr}$ ), cathodic Tafel slope ( $\beta_c$ ), anodic Tafel slope ( $\beta_a$ ), corrosion current density ( $i_{corr}$ ) and the inhibition efficiency  $\eta$  (%) are given in Table 5. It is apparent from the data in Table 5 that the benzimidazole get adsorbed on the carbon steel surface at all temperatures studied (the  $\eta$  (%) is 86% at 333 K).

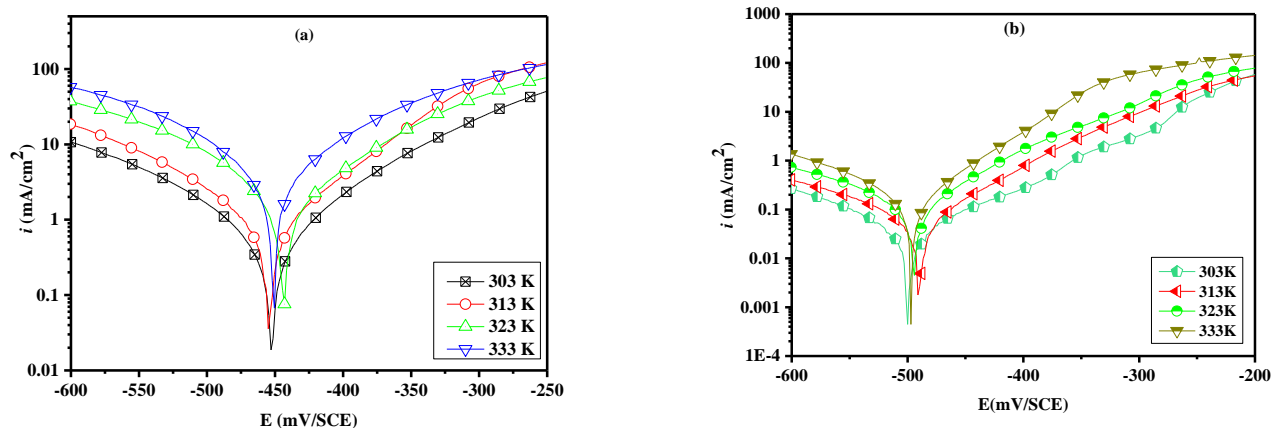


**Figure 5:** Potentiodynamic polarization curves for corrosion of carbon steel in 1M HCl solution in the absence and presence of  $10^{-3}$ M of MSB at different temperatures.

**Table 5.** The results of the temperature effect of carbon steel corrosion performed in 1 M HCl and with  $1 \times 10^{-3}$  M of MSB.

Medium	Temp (K)	$E_{corr}$ (mV/SCE)	$i_{corr}$ ( $\mu\text{A cm}^{-2}$ )	$\eta$ (%)	$\theta$
Blank	303	-452	507	-	-
	313	-454	860	-	-
	323	-443	1840	-	-
	333	-450	2800	-	-
MSB	303	-453	32	94	0.94
	313	-497	80	91	0.91
	323	-518	185	90	0.90
	333	-541	381	86	0.86

The corrosion reaction can be regarded as an Arrhenius-type process; the rate is given by(7) [58]:

$$i_{corr} = k \exp\left(-\frac{E_a}{RT}\right) \quad (7)$$

where  $E_a$  is the apparent activation corrosion energy,  $R$  is the universal gas constant and  $k$  is the Arrhenius pre-exponential constant.

Arrhenius plots for the corrosion density of carbon steel in the case of tested inhibitor are given in Figure 6. Values of apparent activation energy of corrosion ( $E_a$ ) for carbon steel in 1 M HCl with the absence and presence of inhibitor were determined from the slope of  $\ln(i_{corr})$  versus  $1/T$  plots and shown in Table 6. The analysis of the obtained result indicates that  $E_a$  values in presence of inhibitor were higher than that obtained in the case of uninhibited solution (blank). This behavior can suggest that higher energy barrier for the corrosion process in the inhibited solutions[6,8].

Activation parameters like enthalpy ( $\Delta H_a$ ) and entropy ( $\Delta S_a$ ) for the dissolution of carbon steel in 1 M HCl in the absence and presence of  $1 \times 10^{-3}$  M of benzimidazole derivate were calculated from the transition state equation[58]:

$$i_{corr} = \frac{RT}{Nh} \exp\left(\frac{\Delta S_a}{R}\right) \exp\left(-\frac{\Delta H_a}{RT}\right) \quad (8)$$

where  $h$  is Planck's constant,  $N$  is the Avogadro number,  $R$  is the universal gas constant,  $\Delta H_a$  is the enthalpy of activation and  $\Delta S_a$  is the entropy of activation. Figure 7 shows that the Arrhenius plots of  $\ln(i_{corr}/T)$  versus  $1/T$  gave straight lines with slope( $-\Delta H_a/R$ ) and intercept ( $\ln R/Nh + \Delta S_a/R$ ) from where  $\Delta H_a$  and  $\Delta S_a$  values were calculated. The activation parameters are given in Table 6. The higher value of  $\Delta H_a$  indicates creation of energy barrier for the corrosion reaction in presence of inhibitor. The higher value of  $\Delta S_a$  is for inhibited solution might be the result of the adsorption of inhibitor molecules from solution, which could be regarded as a quasi-substitution[59].

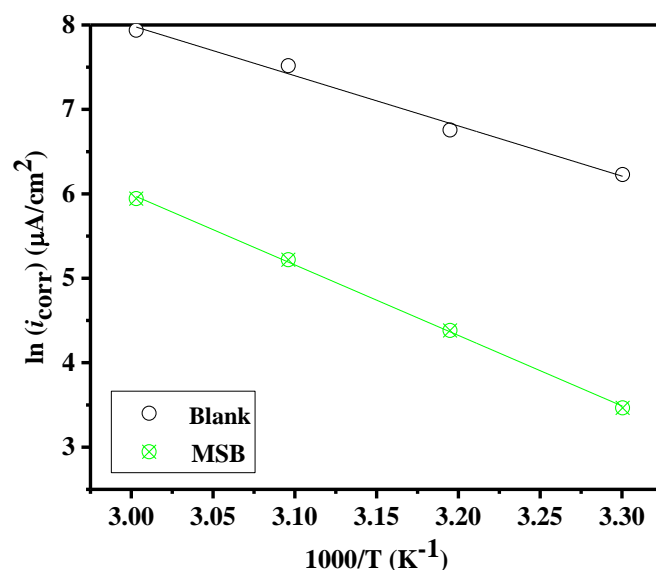


**Figure 6:** Arrhenius plots of  $\ln i_{\text{corr}}$  vs.  $1/T$  for carbon steel in 1M HCl in the absence and the presence of MSB at optimum concentration.

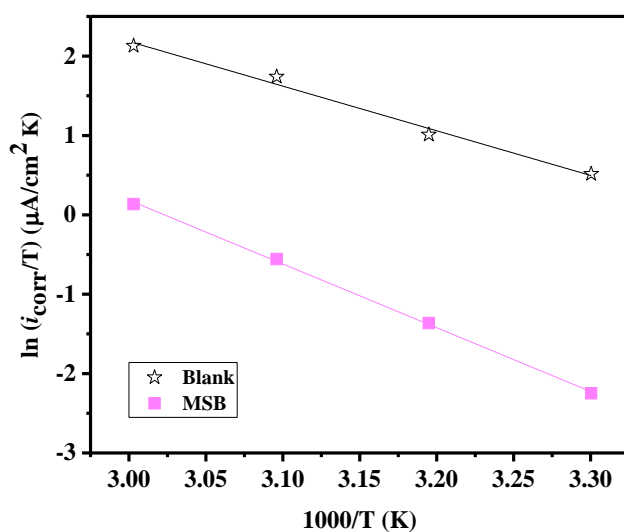


**Figure 7:** Relation between  $\ln (i_{\text{corr}}/T)$  and  $1000/T$  at different temperatures.

**Table 6.** Activation parameters for the carbon steel dissolution in 1M HCl in the absence and the presence of  $10^{-3}\text{M}$  of MSB.

Medium	$E_a$ (kJ mol <sup>-1</sup> )	$\Delta H_a$ (kJ mol <sup>-1</sup> )	$\Delta S_a$ (J mol <sup>-1</sup> K <sup>-1</sup> )
Blank	49.38	46.77	-38.96
MSB	69.43	66.79	4.45

### 3.5. Theoretical calculation:

Quantum chemical calculations were done in order to discuss the adsorption mode through light on the inhibitor molecular structure. Quantum chemical parameters such as  $E_{\text{HOMO}}$ ,  $E_{\text{LUMO}}$ ,  $\Delta E$  and  $\Delta N$  are given in Table 7. The optimized and frontier molecular orbital structures of MSB are shown in Fig. 8. In general, the

donor and acceptor tendency of a molecule is given by  $E_{\text{HOMO}}$  and  $E_{\text{LUMO}}$  values. The higher value of  $E_{\text{HOMO}}$  would be its electron donating ability to the metal. And the higher value of  $E_{\text{LUMO}}$  would be its electron accepting ability from the metal [60]. The energy gap  $\Delta E$ , is an important parameter which indicates the reactivity tendency of organic molecule towards the metal surface, lower the  $\Delta E$  value easier would be the electron transfer from inhibitor to metal [61]. As can be see, the molecular orbitals were distributed almost of the entire molecules, which can assist the neutral and protonated compound to interact more with the carbon steel surface.

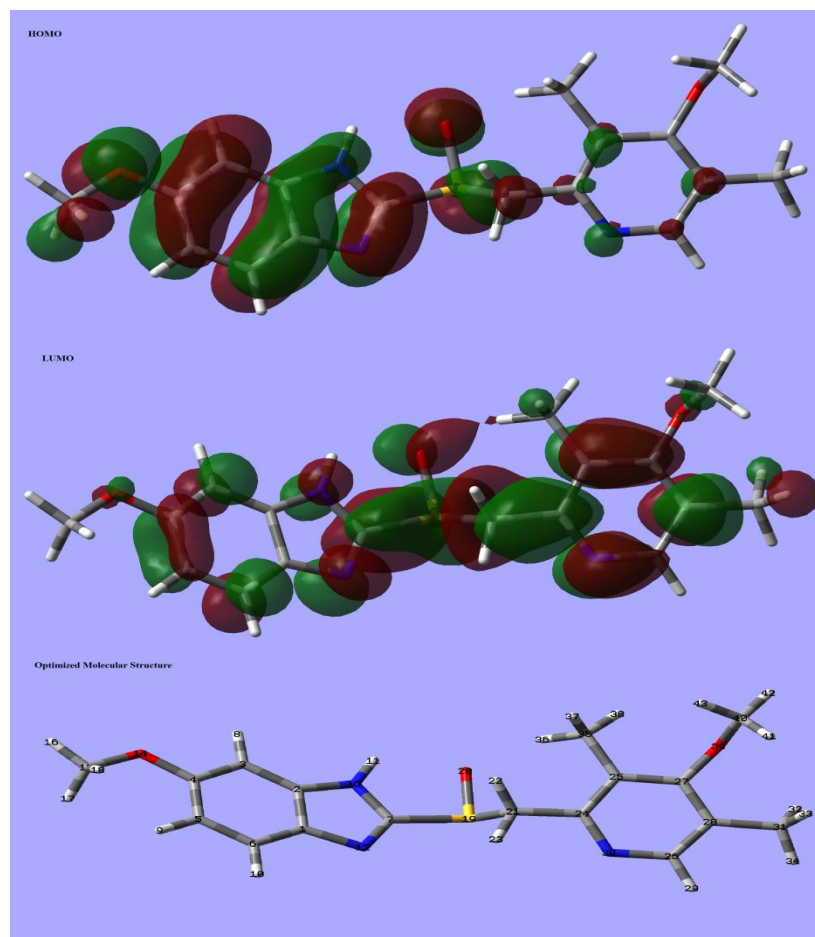


**Figure 8:** Quantum chemical results of inhibitor molecule calculated at DFT/B3LYB/6-31G (d, p)

The quantum chemical calculations parameters such as;  $E_{\text{HOMO}}$ ,  $E_{\text{LUMO}}$ ,  $\Delta E$  and  $\Delta N$  are represented in Table 7. The electron affinity (EA) and ionization potential (IP) are deduced from  $E_{\text{HOMO}}$  and  $E_{\text{LUMO}}$  by the Equations (9) and (10) [62]:

$$\text{IP} = -E_{\text{HOMO}} \quad (9)$$

$$\text{EA} = -E_{\text{LUMO}} \quad (10)$$

Mulliken electronegativity ( $\chi$ ) and Absolute hardness ( $\eta$ ) can be approximated using [63,64]:

$$\chi = \frac{\text{IP} + \text{EA}}{2} \quad (11)$$

$$\eta = \frac{\text{IP} - \text{EA}}{2} \quad (12)$$

The number of transferred electrons ( $\Delta N$ ) is calculated by application of the Pearson method using the equation[65](13):

$$\Delta N = \frac{\Phi - \chi_{\text{inh}}}{2(\eta_{\text{Fe}} + \eta_{\text{inh}})} \quad (13)$$

where  $\Phi$  is the work function of the iron surface with the value of 4.82 eV for Fe (1 1 0) [66,67],  $\chi_{\text{inh}}$  is the absolute electronegativity associated to the inhibitor molecule,  $\eta_{\text{Fe}} = 0$  and  $\eta_{\text{inh}}$  are the absolute hardness of metal and the inhibitor molecule, respectively [68,69].

The energy values of highest occupied molecular orbital ( $E_{\text{HOMO}}$ ), energy of lowest unoccupied molecular orbital ( $E_{\text{LUMO}}$ ) and the separation energy ( $E_{\text{LUMO}}-E_{\text{HOMO}}$ ,  $\Delta E$ ) are also presented in Table 7. High value of  $E_{\text{HOMO}}$  indicates a tendency of the molecule to donate electrons to act with acceptor molecule with low-energy, empty molecular orbital[70]. Similarly,  $E_{\text{LUMO}}$  represents the ability of the molecule to accept electrons, and the lower value of  $E_{\text{LUMO}}$  suggests the molecule accepts electrons more probable[31].

In the same way, the difference between LUMO and HOMO energies ( $\Delta E_{\text{gap}}$ ) is considered as the essential descriptor of the reactivity of an inhibitor, the least  $\Delta E$  (4.42 eV) value, can explain the good inhibition property of tested inhibitor [71]. It has also reported that the  $\Delta N$  value measures the ability of a chemical compound to transfer its electrons to metal if  $\Delta N > 0$  and vice versa if  $\Delta N < 0$  [72,73]. In this study, the positive value of  $\Delta N = 0.311$  presented in Table 7, suggest the high capability of MSB to donates electrons to the CS surface.

**Table 7.** Quantum theoretical parameters for MSB calculated using DFT.

$E_{\text{HOMO}}$	$E_{\text{LUMO}}$	$\Delta E$	$\Delta N$
(eV)	(eV)	(eV)	
-5.65	-1.23	4.42	0.311

### 3.6. Monte Carlo Simulations

Electronic properties alone are not sufficient to predict the trend of the inhibition performance of the investigated inhibitor in spite of its success in exploring the mechanism of inhibitor. Therefore, it is imperative to carry out rigorous modeling of the direct interaction of the inhibitor with steel. Monte Carlo simulations were performed on a system comprising inhibitor molecule and steel surface. Figure 9 represents the most stable low energy configuration for the adsorption of benzimidazole derivative on Fe (110) surface obtained through the Monte Carlo simulations.

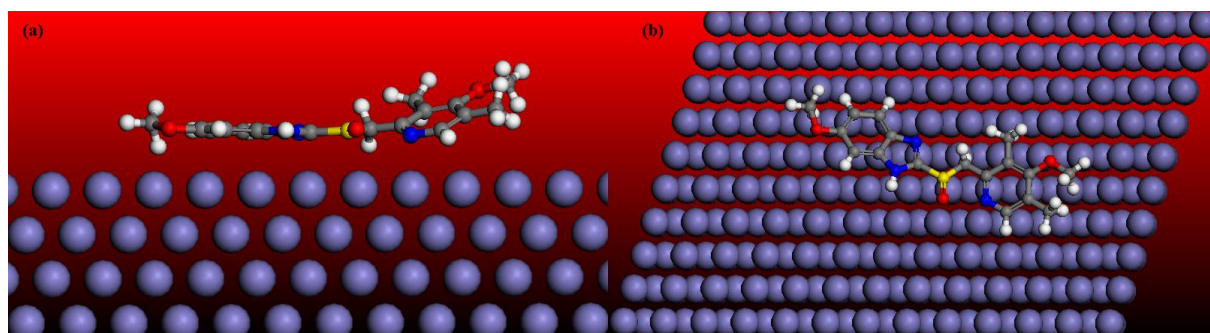


**Figure 9:** The side (a) and top (b) views of the most stable low energy configuration for the adsorption of the inhibitor on Fe (110) surface obtained through the Monte Carlo simulation for MSB.

Several outputs and descriptors calculated by the Monte Carlo simulation are presented in Table 8. The parameters presented in Table 8 include total energy, in  $\text{kcal mol}^{-1}$ , of the substrate–adsorbate configuration. The total energy is defined as the sum of the energies of the adsorbate components, the rigid adsorption energy and the deformation energy. In this study, the substrate energy (iron surface) is taken as zero. In addition, adsorption energy in  $\text{kcal mol}^{-1}$  reports energy released (or required) when the relaxed adsorbate components are adsorbed on the substrate. The adsorption energy is defined as the sum of the rigid adsorption energy and the deformation energy for the adsorbate components. The rigid adsorption energy reports the energy, in  $\text{kcal mol}^{-1}$ , released (or required) when the unrelaxed adsorbate components (i.e., before the geometry optimization step) are adsorbed on the substrate. The deformation energy reports the energy, in  $\text{kcal mol}^{-1}$ , released when the adsorbed adsorbate components are relaxed on the substrate surface. Table 8 shows also ( $dE_{\text{ads}}/dNi$ ), which reports the energy, in  $\text{kcal mol}^{-1}$ , of substrate–adsorbate configurations where one of the adsorbate components has been removed.

It is seen in Table 8, that MSB molecule shows high negative adsorption energy of adsorption ( $-534.06 \text{ kcal mol}^{-1}$ ) during the simulation process. High negative adsorption energy indicates a stable and a stronger adsorption of the inhibitor on metal surface [5]. Thus, the studied inhibitor is likely to adsorb on the steel surface to form stable adsorption layers and protect the carbon steel from corrosion.

**Table 8.** Outputs and descriptors calculated by the Monte Carlo simulation for the lowest adsorption. Configurations of MSB Fe (110) surface (in kcal/mol).

System	Total energy	Adsorption energy	Rigid adsorption energy	Deformation energy	$dE_{ad}/dNi$ inhibitor
Fe (110)/ MSB	-89.12	-534.06	-530.32	3.74	-534.06

### 3.6. The potential of zero charge:

Adsorption of heterocyclic inhibitors on a corroding metal depends mainly on the charge of the metal surface, the dipole moment of heterocyclic inhibitors, and the adsorption of other ionic species if it is electrostatic in nature. The potential of zero charge (PZC) plays a very important role in the electrostatic adsorption process. The surface charge of the metal can be examined by comparing the potential of open circuit potential ( $E_{OCP}$ ) of carbon steel containing solution with potential of zero charge ( $E_{PZC}$ ) (the minimum  $C_{dl}$  value). After 30min of immersion in 1M HCl solution with 1mM MSB, we were characterized by the plot of  $C_{dl}$  in Fig. 10.

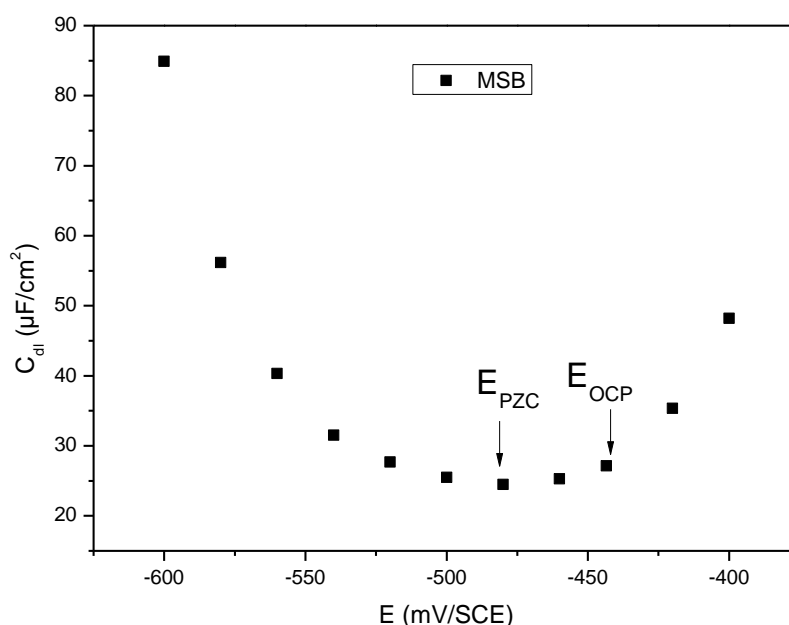


**Figure 10:** the plot of  $C_{dl}$  versus electrode potential for CS containing 10.0 Mm MSB in 1.0 M HCl.

In this work, we can show that the potential of zero charge (PZC) is -480 mV/SCE) which is more negative than the corrosion potential is - 445 mV/SCE (Fig.10). This result reveals that the carbon steel surface carries an excess positive charge [74].

## Conclusion

The investigated benzimidazole derivative (MSB) show excellent inhibition efficiency for CS in 1 M HCl. Polarization study reveals that MSB act as mixed-type inhibitor but predominantly shift in cathodic direction. Electrochemical impedance spectroscopy experiments have shown that an increase in inhibitor concentration causes an increase in polarisation resistance  $R_p$  and a decrease in  $C_{dl}$  value, owing to the increased thickness of the adsorbed layer. The experimental inhibition has supported by the theoretical calculations results, which affirmed the highest inhibition efficiency of MSB molecule. The adsorption of the inhibitor molecule on the carbon steel surface was found to obey the Langmuir adsorption isotherm. The calculated adsorption energy by Monte Carlo simulations reveals the possible adsorption of studied compound through heteroatoms.

## References

1. El Makrini B., Lgaz H., Larouj M., Salghi R., Rasem Hasan A., Belkhaouda M., Jodeh S., Zougagh M., Oudda H., *Pharma. Chem.* 8 (2016) 256.
2. Krim O., Krim O., Messali M., Hammouti B., Elidrissi A., Khaled K., Salghi R., Lgaz H., *Port. Electrochimica. Acta.* 34 (2016) 213.
3. El Aoufir Y., Lgaz H., Bourazmi H., Kerroum Y., Ramli Y., Guenbour A., Salghi R., El-Hajjaji F., Hammouti B., Oudda H., *J. Mater. Environ. Sci.* 7 (2016) 4330.
4. El Aoufir Y., Lgaz H., Toumiat K., Salghi R., Jodeh S., Zougagh M., Guenbour A., Oudda H., *Res. J. Pharm. Biol. Chem. Sci.* 7 (2016) 1219.
5. Toumiat K., El Aoufir Y., Lgaz H., Salghi R., Jodeh S., Zougagh M., Oudda H., *MRes. J. Pharm. Biol. Chem. Sci.* 7 (2016) 1209.
6. Verma C., Quraishi MA., Singh A., *J. Mol. Liq.* 212 (2015) 804–812.
7. Singh DK., Kumar S., Udayabhanu G., John RP., *J. Mol. Liq.* 216 (2016) 738.
8. Verma C., Ebenso EE., Bahadur I., Obot IB., Quraishi MA., *J. Mol. Liq.* 212 (2015) 209.
9. Yadav M., Sinha RR., Sarkar TK., Bahadur I., Ebenso EE., *J. Mol. Liq.* 212 (2015) 686.
10. Tawfik SM., *J. Mol. Liq.* 207 (2015) 185.
11. Ghazoui A., Zarrouk A., Bencat N., Salghi R., Assouag M., El Hezzat M., Guenbour A., Hammouti B., *J. Chem. Pharm. Res.* 6 (2014) 704.
12. Zarrok H., Zarrouk A., Salghi R., Ramli Y., Hammouti B., Al-Deyab S.S., Essassi E.M., Oudda H., *Int. J. Electrochem. Sci.* 7(9) (2012) 8958.
13. Bendaha H., Zarrouk A., Aouniti A., Hammouti B., El Kadiri S., Salghi R., Touzan R., *Phys. Chem. News* 64 (2012) 95.
14. Zarrouk A., Hammouti B., Zarrok H., Salghi R., Dafali A., Bazzi L., Bammou L., Al-Deyab S.S., *Der Pharm. Chem.* 4(1) (2012) 337.
15. Ghazoui A., Saddik R., Benchat N., Hammouti B., Guenbour M., Zarrouk A., Ramdani M., *Der Pharm. Chem.* 4(1) (2012) 352.
16. Zarrouk A., Hammouti B., Zarrok H., Bouachrine M., Khaled K.F., Al-Deyab S.S., *Int. J. Electrochem. Sci.* 6 (2012) 89.
17. Zarrok H., Zarrouk A., Salghi R., Assouag M., Hammouti B., Oudda H., Boukhris S., Al Deyab S.S., Warad I., *Der Pharm. Lett.* 5(2) (2013) 43.
18. Zarrok H., Saddik R., Oudda H., Hammouti B., El Midaoui A., Zarrouk A., Benchat N., Ebn Touhami M., *Der Pharm. Chem.* 3(5) 2011) 272.
19. Zarrouk A., Hammouti B., Touzani R., Al-Deyab S.S., Zertoubi M., Dafali A., Elkadiri S., *Int. J. Electrochem. Sci.* 6 (10) (2011) 4939.
20. Adardour L., Lgaz H., Salghi R., Larouj M., Jodeh S., Zougagh M., Hamed O., Taleb M., *Pharm. Lett.* 8 (2016) 173.
21. Adardour L., Lgaz H., Salghi R., Larouj M., Jodeh S., Zougagh M., Warad I., Oudda H., *Pharm. Lett.* 8 (2016) 126.
22. El Makrini B., Toumiat K., Lgaz H., Salghi R., Jodeh S., Hanbali G., Belkhaouda M., Zougagh M., *Res. J. Pharm. Biol. Chem. Sci.* 7 (2016) 2286.
23. Lgaz H., Salghi R., Jodeh S., Hammouti B., Effect of clozapine on inhibition of mild steel corrosion in 1.0 M HCl medium. *J. Mol. Liq.* 225 (2017) 271.
24. Toumiat K., El Aoufir Y., Lgaz H., Salghi R., Jodeh S., Zougagh M., Oudda H., *Res. J. Pharm. Biol. Chem. Sci.* 7 (2016) 1210.
25. Saadouni M., Larouj M., Salghi R., Lgaz H., Jodeh S., Zougagh M., Souzizi A., *Pharm. Lett.* 8 (2016) 96.
26. El Aoufir Y., Lgaz H., Toumiat K., Salghi R., Jodeh S., Zougagh M., Guenbour A., Oudda H., *Res. J. Pharm. Biol. Chem. Sci.* 7 (2016) 1200.
27. Popova A., Sokolova E., Raicheva S., Christov M., *Corros. Sci.* 45 (2003) 33.
28. Popova A., Christov M., Raicheva S., Sokolova E., *Corros. Sci.* 46 (2004) 1333.
29. Popova A., Christov M., *Corros. Sci.* 48 (2006) 3208.
30. Benabdellah M., Tounsi A., Khaled K.F., Hammouti B., *Arab. J. Chem.* 4 N°1(2011)17-24.
31. Ghanbari A, Attar M, Mahdavian M. *Mater. Chem. Phys.* 124 (2010) 1205.
32. Khaled K., *Electrochimica Acta* 48 (2003) 2493.
33. Sachs G., Chang H.H., Rabon E., Schackman R., Lewin M., Saccomani G., *J. Biol. Chem.* 251 (1976) 7690
34. Dibona D.R., Ito S., Berglinth T., Sachs G., *Proc. Natl. Acad. Sci. U. S. A.* 76 (1979) 6689.

35. Fellenius E., Berglindh T., Sachs G., *Nature* 290 (1981) 156.
36. Frisch M.J., Trucks G.W., Schlegel H.B., Scuseria G.E., Robb M.A., Cheeseman J.R., Montgomery J.A., Jr., Vreven T., Kudin K.N., Burant J.C., Millam J.M., S.S. Iyengar, J. Tomasi, V. Barone, B. Mennucci, M. Cossi, G. Scalmani, N. Rega, G.A. Petersson, H. Nakatsuji, M. Hada, M. Ehara, K. Toyota, R. Fukuda, J. Hasegawa, M. Ishida, T. Nakajima, Y. Honda, O. Kitao, H. Nakai, M. Klene, X. Li, J. E. Knox, H.P. Hratchian, J.B. Cross, V. Bakken, C. Adamo, J. Jaramillo, R. Gomperts, R. E. Stratmann, O. Yazyev, A.J. Austin, R. Cammi, C. Pomelli, J.W. Ochterski, Ayala P.Y., Morokuma K., Voth G.A., P. Salvador, J.J. Dannenberg, V.G. Zakrzewski, S. Dapprich, Daniels A.D., M. C. Strain, O. Farkas, D. K. Malick, A.D. Rabuck, K. Raghavachari, J.B. Foresman, J.V. Ortiz, Q. Cui, A.G. Baboul, S. Clifford, J. Cioslowski, B.B. Stefanov, G. Liu, A. Liashenko, P. Piskorz, I. Komaromi, R.L. Martin, D. J. Fox, T. Keith, M.A. Al-Laham, C.Y. Peng, A. Nanayakkara, M. Challacombe, Gill P.M.W., B. Johnson, W. Chen, M. W. Wong, C. Gonzalez, and J. A. Pople., Gaussian 03, Revision C.02.
37. Lee C., Yang W., Parr R.G., *Phys. Rev. B* 37 (1988) 785.
38. Materials Studio. *Revision 6.0*. Accelrys Inc., San Diego, USA (2013).
39. Verma C., Ebenso E.E., Bahadur I., Obot I.B., Quraishi M.A., *J. Mol. Liq.* 212 (2015) 209.
40. Obot I.B., Kaya S., Kaya C., Tüzün B., *Phys. E. Low-Dimens. Syst. Nanostructures*. (2016) doi: 10.1016/j.physe.2016.01.024
41. Kaya S., Tüzün B., Kaya C., Obot I.B., *J. Taiwan. Inst. Chem. Eng.* 58 (2016) 528.
42. Verma C., Ebenso E.E., Olasunkanmi L.O., Quraishi M.A., Obot I.B., *J. Phys. Chem. C*, 120 (2016) 11598
43. Fu J., Pan J., Liu Z., Li S., Wang Y., *Int. J. Electrochem. Sci.* 6 (2011) 2072.
44. Mistry B.M., Jauhari S., *Res. Chem. Intermed.* 39 (2013) 1049.
45. Haque J., Srivastava V., Verma C., Quraishi M.A., *J. Mol. Liq.* 225 (2017) 848.
46. Solmaz R., Kardaş G., Culha M., Yazıcı B., Erbil M., *Electrochim Acta* 53 (2008) 5941.
47. Erbil M., *Chimica Acta Turcica* 1 (1988) 59.
48. Ghazoui A., Benchat N., El-Hajjaji F., Taleb M., Rais Z., Saddik R., Elaatioui A., Hammouti B., *Journal of Alloys and Compounds*, 693 (2017) 510-517
49. Amin M.A., El-Rehim S.A., El-Sherbini E., Bayoumi R.S., *Int. J. Electrochem. Sci.* 3 (2008) 199.
50. Youse A., Javadian S., Dalir N., Kakemam J., Akbari J., *RSC Adv.*, 5 (2015) 11697.
51. Verma C., Quraishi M.A., Singh A., *J. Taibah Univ.* 10 (2016) 718.
52. Tang Y., Zhang F., Hu S., Cao Z., Wu Z., Jing W., *Corros. Sci.* 74 (2013) 271.
53. Verma C., Quraishi M.A., Ebenso E.E., Obot I.B., El Assyry A., *J. Mol. Liq.* 219 (2016) 647.
54. Lgaz H., Salghi R., Jodeh S., Toumiat K., Larouj M., *Appl J Environ. Eng. Sci.* 1 (2015) 57.
55. Lgaz H., Toumiat K., Jodeh S., Salghi R., *Appl. J. Environ. Eng. Sci.* 2 (2016) 72.
56. Bousskri A., Anejjar A., Lgaz H., Belkhaouda M., Jodeh S., Hammouti B., *Appl. J. Environ. Eng. Sci.* 1 (2015) 9.
57. Verma C, Quraishi MA, Ebenso EE, Obot IB, El Assyry A. *J. Mol. Liq.* 219 (2016) 647.
58. Bahrami M.J., Hosseini S.M.A., Pilvar P., *Corros. Sci.* 52 (2010) 2793.
59. Tao Z., He W., Wang S., Zhang S., Zhou G., *Corros. Sci.* 60 (2012) 205.
60. Singh R.N., Kumar A., Tiwari R.K., Rawat P., *Spectrochim Acta A Mol Biomol Spectrosc* 112(2013) 182.
61. Daoud D., Douadi T., Hamani H., Chafaa S., Al-Noaimi M., *Corros Sci.* 94 (2015) 21.
62. Jafari H., Danaee I., Eskandari H., RashvandAvei M., *J. Mater. Sci. Technol.* 30 (2014) 239.
63. Pearson R.G., *Inorg. Chem.* 27 (1988) 734.
64. Sastri V., Perumareddi J., *Corros. Sci.* 53 (1997) 617.
65. Martinez S., *IMater. Chem. Phys.* 77 (2003) 97.
66. Lukovits I., Kalman E., Zucchi F., *Corros. Sci.* 57 (2001) 3.
67. Pearson R.G., *Inorg Chem.* 27 (1988) 734.
68. Cao Z., Tang Y., Cang H., Xu J., Lu G., Jing W., *Corros. Sci.* 83 (2014) 292.
69. Kokalj A., *Chem. Phys.* 393 (2012) 1.
70. Lgaz H., Rachid S., Larouj M., Elfaydy M., Jodeh S., Abbout H., Lakhrissi B., Toumiat K., Oudda H., *Mor. J. Chem.* 4 N°2 (2016) 592.
71. Yadav M, Kumar S., Bahadur I., Ramjugernath D., *Int. J. Electrochem. Sci.* 9 (2014) 3928.
72. Kokalj A., *Electrochimica. Acta.* 56 (2010) 745.
73. Kovačević N., Kokalj A., *Corros. Sci.* 53 (2011) 909.
74. Zang K., Xu B., Yang W. Yin X., Liu X., Chen Y., *Corros. Sci.* 90 (2015) 284.

(2017) ; <http://www.jmaterenvironsci.com>